Research Article

# Rapid Visual CRISPR Assay: A Naked-Eye Colorimetric Detection Method for Nucleic Acids Based on CRISPR/Cas12a and a Convolutional Neural Network

Shengsong Xie,[○] Dagang Tao,[○] Yuhua Fu,[○] Bingrong Xu,[○] You Tang, Lucilla Steinaa, Johanneke D. Hemmink, Wenya Pan, Xin Huang, Xiongwei Nie, Changzhi Zhao, Jinxue Ruan, Yi Zhang, Jianlin Han, Liangliang Fu, Yunlong Ma, Xinyun Li,* Xiaolei Liu,* and Shuhong Zhao*

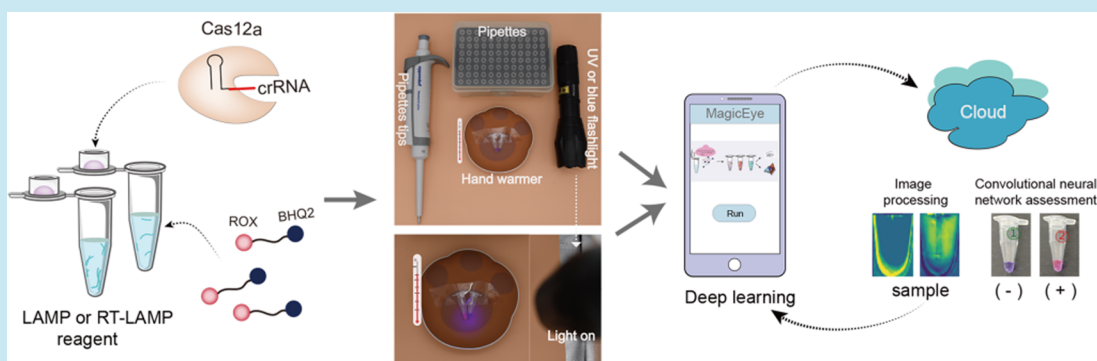Cite This: https://doi.org/10.1021/acssynbio.1c00474

Read Online

ACCESS | Metrics & More | Article Recommendations | Supporting Information

**ABSTRACT:** Rapid diagnosis based on naked-eye colorimetric detection remains challenging, but it could build new capacities for molecular point-of-care testing (POCT). In this study, we evaluated the performance of 16 types of single-stranded DNA-fluorophore-quencher (ssDNA-FQ) reporters for use with clusters of regularly spaced short palindrome repeats (CRISPR)/Cas12a-based visual colorimetric assays. Among them, nine ssDNA-FQ reporters were found to be suitable for direct visual colorimetric detection, with especially very strong performance using ROX-labeled reporters. We optimized the reaction concentrations of these ssDNA-FQ reporters for a naked-eye read-out of assay results (no transducing component required for visualization). In particular, we developed a convolutional neural network algorithm to standardize and automate the analytical colorimetric assessment of images and integrated this into the MagicEye mobile phone software. A field-deployable assay platform named RApid VIsual CRISPR (RAVI-CRISPR) based on a ROX-labeled reporter with isothermal amplification and CRISPR/Cas12a targeting was established. We deployed RAVI-CRISPR in a single tube toward an instrument-less colorimetric POCT format that required only a portable rechargeable hand warmer for incubation. The RAVI-CRISPR was successfully used for the high-sensitivity detection of severe acute respiratory syndrome coronavirus 2 (SARS-CoV-2) and African swine fever virus (ASFV). Our study demonstrates this RAVI-CRISPR/MagicEye system to be suitable for distinguishing different pathogenic nucleic acid targets with high specificity and sensitivity as the simplest-to-date platform for rapid pen- or bed-side testing.

**KEYWORDS:** nucleic acid detection, CRISPR-Cas12a assay, convolutional neural network, MagicEye software

## 1. INTRODUCTION

Nucleic acid-based assays have been widely adopted in many fields, for example, in the diagnosis of infectious diseases,[1] genotyping,[2] and food safety testing.[3] Infectious diseases are presently the focus of considerable research attention to resolve long-standing public health problems, from "classical" diseases to newly emerging epidemic outbreaks. In particular, severe acute respiratory syndrome coronavirus 2 (SARS-CoV-2), the novel RNA virus responsible for the COVID-19 pandemic, has had a major impact on human health worldwide,[4] infecting over 178 million people as of June 2021, as reported to the World Health Organization (WHO) (https://covid19.who.int). To control COVID-19 pandemic, there is an urgent need to test for the SARS-CoV-2 in as many people as possible.[5−7] Similarly, animal production is periodi-

cally subject to widespread viral epidemics, as in the case of African swine fever virus (ASFV), a DNA virus that infects domestic pigs and wild boars with a mortality rate of up to 100%.[8] Although agricultural epidemics receive less attention compared with human epidemics, the early diagnosis of ASFV is necessary to monitor circulating virus for the control and prevention of current and future outbreaks,[9,10] which have major impacts on food production and economy.[11] Although current polymerase chain reaction (PCR)-based clinical diagnostic methods for the detection of viral nucleic acids are highly sensitive, these methods require expensive equipment, trained technicians, and clean laboratory environments, thus limiting their application in developing nations and rural areas without clinical infrastructure.[12]

Thus, increasing the affordability of point-of-care testing (POCT)[13] and moving diagnostic testing for viral pathogens such as SARS-CoV-2 or ASFV from the laboratory to pen- or bed-side detection could be potentially transformative for epidemiological efforts. Although real-time quantitative PCR (qPCR)-based nucleic acid detection is the current gold standard for SARS-CoV-2 and ASFV diagnosis,[14,15] isothermal amplification techniques, such as loop-mediated isothermal amplification (LAMP) and recombinase polymerase amplification (RPA), represent comparatively easy, accessible, and reliable alternatives.[16,17] In particular, these methods can combine a variety of portable read-out types for POCT, such as paper lateral flow test strips or fluorescence and colorimetric assays.[18–20] LAMP/RPA-based detection methods have been rapidly developed and deployed for both SARS-CoV-2 or ASFV owing to their high efficiency of amplification.[21–24] However, a vast majority of these LAMP/RPA-based assays depend on nonspecific nucleic acid detection, meaning that unintended LAMP/RPA amplicons cannot be distinguished from the amplicons of correct targets, leading to unreliable test results.[25,26]

To overcome this issue, nucleic acid detection methods based on a combination of clusters of regularly spaced short palindrome repeats (CRISPR) and LAMP or RPA were developed, including SHERLOCK, DETECTR, HOLMES, and CDetection.[27–30] These diagnostic strategies use Cas proteins, which have collateral nuclease activity to specifically target double-strand DNA (dsDNA) or single-strand RNA (ssRNA) and a protospacer adjacent motif (PAM) sequence, thereby effectively avoiding false-positive results in isothermal amplification.[31,32] In addition, some studies have reported that Cas-based detection methods can distinguish differences at the single nucleotide level by integrating an optimized CRISPR RNA (crRNA),[29,30,33] and several improvements to CRISPR-based detection have been developed for POCT applications, such as CRISPR-based lateral flow strip assay,[34,35] CRISPR-based fluorescent cleavage assay,[36,37] plasmonic CRISPR/Cas12a assay,[38,39] and Cas12a-modulated fluorescence resonance energy transfer assay that incorporates nanomaterials for nucleic acid sensing.[40] Other studies have established methods that seek to simplify the reaction process, such as the All-In-One Dual CRISPR/Cas12a assay[41] and a CRISPR/Cas12a-based portable biosensor.[42] Moreover, mobile phone applications (apps) and mobile phone-based devices have been developed to support the evaluation of lateral flow strips or fluorescence signal read-outs.[43–45] However, there is still a lack of mobile phone software for the colorimetric CRISPR/Cas12a assay.

In this study, to establish an accurate and convenient platform based on the colorimetric detection of viral nucleic acids, we developed a practical POCT detection system that does not require advanced training or specialized instruments. We demonstrated the proof-of-concept in the RApid VIsual CRISPR (RAVI-CRISPR) system for sensitive testing of simulated SARS-CoV-2 and real ASFV infection samples by a naked-eye detection. Especially, we developed a convolutional neural network (CNN) algorithm to standardize and automate the analytical colorimetric assessment of images and integrated this into a MagicEye mobile phone software for the rapid detection of SARS-CoV-2 and ASFV.

## 2. MATERIALS AND METHODS

**2.1. Nucleic Acid Preparation.** The partial fragment 780 bp of ASFV (GenBank accession number: MK333180) *p72* gene that was cloned into the pMD18T vector (Cat. No. D101A, TAKARA, China) was synthesized (TSINGKE, Beijing, China). pBluescript-N vector containing 931 bp of SARS-CoV-2 (GenBank accession number: NC_045512.2) *N* gene was acquired from Fubio (Cat. No. FNV2614, Shanghai, China). The *E* gene (374 bp) of SARS-CoV-2 was synthesized and cloned into the pUC57 vector (TSINGKE, Beijing, China). The *N* gene (235 bp) and *E* gene (563 bp) of SARS-CoV (GenBank accession number: NC_004718.3) were synthesized (TSINGKE, Beijing, China). The *N* gene (232 bp) and *E* gene (249 bp) of Middle East respiratory syndrome coronavirus (MERS-CoV) (GenBank accession number: KT326819.1) were also synthesized (TSINGKE, Beijing, China) (Table S1).

For ASFV, blood samples were collected from pigs before and at different time points of an experimental challenge by ASFV at the International Livestock Research Institute (ILRI), Kenya. DNA was extracted from the ethylenediaminetetra-acetic acid (EDTA)-treated blood samples with the DNeasy Blood & Tissue Kits (Cat. No. 69504, Qiagen, GmBH, Germany) at the BSL2 lab of ILRI. Both qPCR-negative and qPCR-positive samples were selected to test the system.

**2.2. Exonuclease I Cleavage assay.** Sixteen single-stranded DNA-fluorophore-quencher (ssDNA-FQ) reporters, namely, ROX-N12-BHQ2, Texas Red-N12-BHQ2, VIC-N12-BHQ2, JOE-N12-BHQ1, HEX-N12-BHQ1, TAMRA-N12-BHQ2, TET-N12-BHQ1, PET-N12-BHQ1, Alexa Flour 633(NHS)-N12-BHQ2, Quasar 570-N12-BHQ2, Quasar 670-N12-BHQ3, FAM-N12-BHQ1, Cy3-N12-BHQ2, Cy5-N12-BHQ2, Cy5.5-N12-BHQ2, and Cy7-N12-BHQ2, were synthesized (TSINGKE, Beijing, China) for the optimization of their concentration range and gradient in the CRISPR-Cas12a reaction. These ssDNA-FQ reporters that contained a fluorophore at their 5′ end and a matched nonfluorescent quencher at their 3′ end are listed in Table S1. In addition, exonuclease I (Cat. No. M0293S, New England Biolabs (NEB), Ipswich, MA) cleavage was performed for different concentrations of ssDNA-FQ reporters for 15 min at 37 °C on the NaCha Multi-Temp Platform (NaCha, Monad, Suzhou, China). The signals of degraded ssDNA-FQ reporters after the cleavage were detected by both the automatic gel imaging analysis system (Peiqing Science and Technology, Shanghai, China) with UV light and the visible light gel viewer (EP2020, BioTeke, Wuxi, China) with blue light. The background signals and fluorescence intensity of different concentrations of the ssDNA-FQ reporters before and after the cleavage were further measured with the EnSpire Multimode Plate Reader (EnSpire,

PerkinElmer, Waltham, MA). Fluorescence emission and excitation wavelengths were set to 520−770 and 490−750 nm, respectively, which corresponded to the emission and excitation profiles of the ssDNA-FQ reporters.

### 2.3. Design of Target Sites for Virus-Specific crRNAs.
We designed five crRNAs targeting SARS-CoV-2 E and nine crRNAs targeting SARS-CoV-2 N genes by CRISPR-offinder[46] (Table S1). Similarly, a highly active crRNA against the ASFV p72 gene was selected from our previous study.[37]

### 2.4. *In Vitro* RNA Transcription Using T7 RNA Polymerase.
SARS-CoV-2 N and E genes were transcribed from the pBluescript-N and pUC57-E plasmids by adding a T7 promoter *via* PCR using Premix Taq (Cat. No. R004A, TAKARA, Shuzo, Shiga, Japan). The crRNA templates were amplified *via* PCR from a pUC57-T7-crRNA (Table S1) using a forward primer containing T7 promoter and a reverse primer containing the nucleotide target sequences (Table S1). The PCR products were purified using the PCR purification kit (Cat. No. TD407, Beijing Tianmo Sci & Tech Development, Beijing, China). Next, these products were used as the DNA templates for in vitro transcription reactions with the HiScribe T7 High Yield RNA Synthesis Kit (Cat. No. E2040S, NEB). DNA templates were removed by the addition of DNase I (Cat. No. M0303S, NEB) at 37 °C for 15 min. Subsequently, in vitro-transcribed RNA was purified using the Monarch RNA Cleanup Kit (Cat. No. T2040S, NEB). RNA concentration was quantified with a NanoDrop 2000 spectrophotometer (Thermo Fisher Scientific, Wilmington, DE). The copy number was calculated according to their concentration and transcript length.

### 2.5. Real-Time (RT)-qPCR/qPCR Assay.
Different copies of RNA transcribed in vitro from SARS-CoV-2 N and E genes were quantified *via* RT-qPCR. The probes, primers, and their relative concentrations were designed according to the suggestions of the Centers for Disease Control and Prevention (CDC) and World Health Organization (WHO) (Table S1). The Luna Universal Probe One-Step RT-qPCR Kit (Cat. No. E3006S, NEB) was used as the relevant master mix. RT-qPCR reaction components and the thermocycling conditions were according to the CDC and WHO protocol, using a cycle threshold (Ct) value >40 as negative.[47,48] Similarly, the qPCR assay and primers (Table S1) for the detection of ASFV p72 followed the reaction conditions recommended by the World Organisation for Animal Health (OIE), using a Ct value >35 as negative.[49] SYBR Green Realtime PCR Master Mix (Cat. No. QPK-201, Toyobo, Osaka, Japan) was used as the relevant master mix. The qPCR reaction was performed in the CFX96 Touch Real-Time PCR Detection System (Bio-Rad, Hercules, CA).

### 2.6. RAVI-CRISPR Assays with RT-LAMP/LAMP.
RT-LAMP/LAMP primers (Table S1) used for the amplification of the 238 bp N gene fragment and 200 bp E gene fragment of SARS-CoV-2 as well as the 198 bp fragment of the ASFV p72 gene were designed using PrimerExplorer V5 (https://primerexplorer.jp/e/). ASFV p72-containing plasmid was serially diluted from $7 \times 10^5$ to $7 \times 10^{-1}$ copies/μL. In vitro-transcribed N gene RNA of SARS-CoV-2 was diluted from $4 \times 10^5$ to $4 \times 10^{-1}$ copies/μL, and in vitro-transcribed E gene RNA of SARS-CoV-2 was diluted from $5.8 \times 10^4$ to $5.8 \times 10^{-1}$ copies/μL. According to the manufacturer's instructions, the RT-LAMP/LAMP assays were performed in a 25 μL system. The reaction mixture containing 1× isothermal amplification buffer, 1 μL of Bst 3.0 DNA polymerase (Cat. No. M0374L,

NEB), 1.4 mM dNTP Mix, 6 mM $MgSO_4$, 1.6 μM FIP/BIP primers, 0.2 μM F3/B3 primers, 0.4 μM LF/LB primers, and 1 μL of different input synthesized RNA/plasmid templates or 2 μL of input DNA from a pig blood sample. The amplification reactions were performed at 65 °C for 40 min in the NaCha Multi-Temp Platform. Then, 3 μL of each product was used for RAVI-CRISPR assays, and 3 μL of the remaining products was used for 2% agarose gel electrophoresis.

EnGen Lba Cas12a (Cat. No. M0653S, NEB) and NEBuffer 2.1 (Cat. No. B7202S, NEB) were purchased from the NEB. Twenty microliters of the RAVI-CRISPR assay contained 500 nM Cas12a, 2 μL of NEBuffer 2.1, 1 μM crRNA, 20 μM ssDNA-FQ reporter (ROX-N12-BHQ2), and 3 μL of preamplified products. The reaction was performed at 37 °C. Then, PCR tubes containing 20 μL of the RAVI-CRISPR test samples were placed on a black board (under no excitation light) or under a blue/UV light transilluminator for the naked eye or fluorescence visualization. A smartphone camera or the Peiqing automatic gel imaging analysis system in the same exposure time recorded the results. For fluorescence intensity measurement using the EnSpire Multimode Plate Reader, 2.5 μM ssDNA-FQ reporters were added to the tubes, and fluorescence excitation and emission wavelengths were set to 576 and 601 nm, respectively. For lateral flow visual detection, 2.5 μM ssDNA-FQ (FAM-N12-Biotin) reporter was added to the tube, followed by the treatment with the HybriDetect—Universal Lateral Flow Assay Kit (Milenia Biotec, Gießen, Germany), and the result was visualized after approximately 5 min.

### 2.7. Single-Tube RAVI-CRISPR Assay.
Single-tube RAVI-CRISPR assay was conducted using components A and B. Component A contained 1× isothermal amplification buffer, 1 μL of Bst 3.0 DNA polymerase (Cat. No. M0374L, NEB), 1.4 mM dNTP Mix, 6 mM $MgSO_4$, 1.6 μM FIP/BIP primers, 0.2 μM F3/B3 primers, and 0.4 μM LF/LB primers. Component B contained 500 nM Cas12a, 1 μM crRNA, and 2 μL of NEBuffer 2.1. For the 25 μL of single-tube RAVI-CRISPR assay, component A was first added to the bottom of the PCR tube. Then, the amplified template mixed with 20 μM ssDNA-FQ (ROX-N12-BHQ2) reporter was added to the PCR tube and vortexed to mix. Next, 1.6 μL of mineral oil was added to the bottom liquid for insulation, then 5 μL of component B was placed in the lid, and PCR was carried for 40 min at 65 °C. Afterward, the PCR tube was mixed thoroughly and reacted at 37 °C for 15 min. All incubation reactions were performed on the portable rechargeable hand warmer, which provided temperatures from 35 to 60 °C. For the naked eye or fluorescence visualization, PCR tubes containing 25 μL of single-tube RAVI-CRISPR reaction solution were checked under blue or UV light.

### 2.8. Image Identification and Segmentation in PCR Tubes.
A single deep neural network (https://github.com/bubbliiiing/ssd-keras)[50] was used to identify the images of PCR tubes, and the detection models were trained based on the TensorFlow (v1.13.1) and Keras (v2.1.5) frameworks.[51,52] The images captured under no excitation light were used to train the PCR tube recognition models. Single-PCR tubes and eight-tube PCR strips were used to improve the generalization power of the models. In addition, functions in the opencv-python (v4.4.0.46) library (https://github.com/opencv/opencv-python), namely, "median blur operation", "opening operation", "closing operation", "binary thresholding operation", "kmeans", "PCACompute2", and "findContours", were
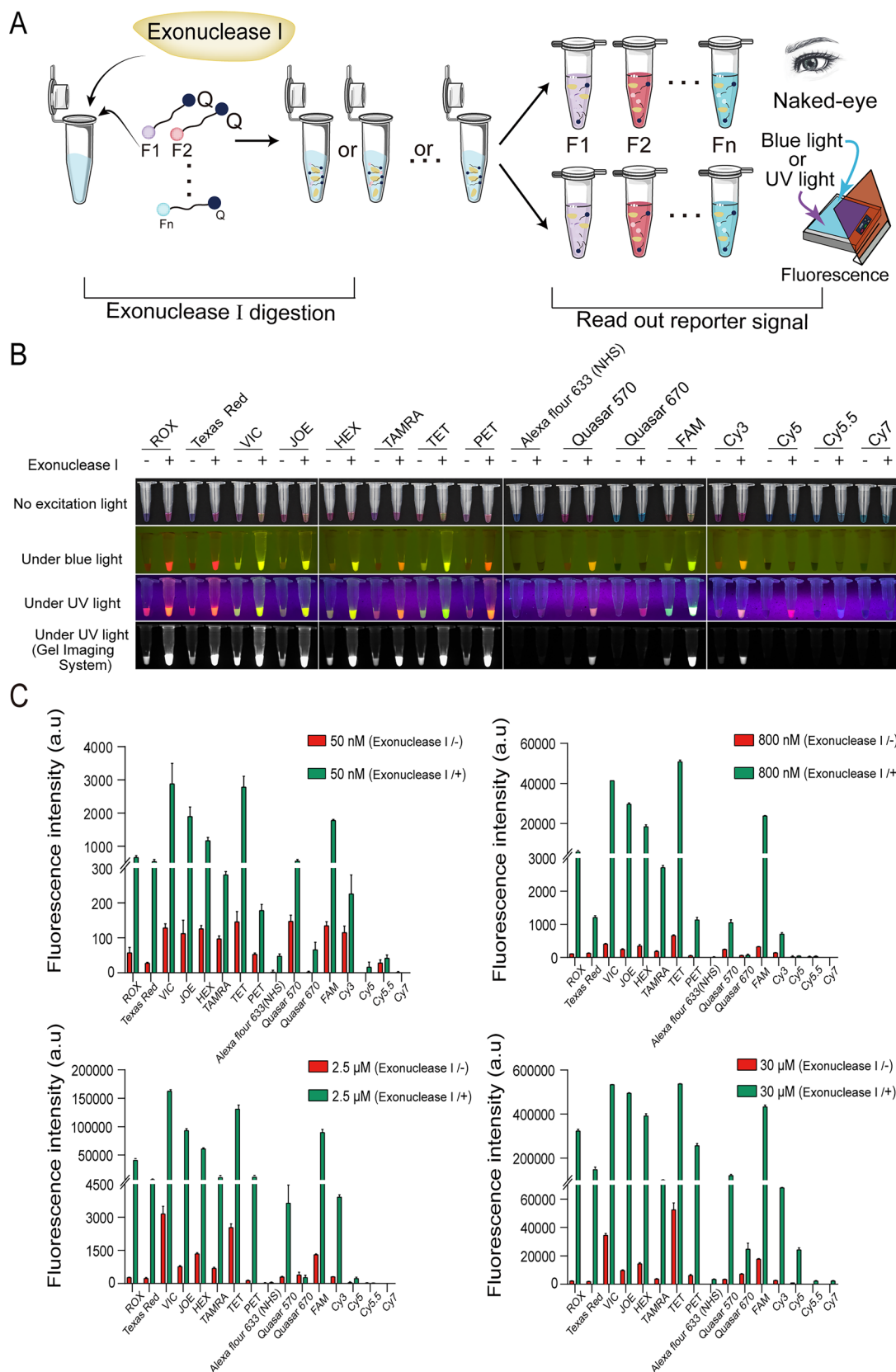
**Figure 1.** Screening and optimization of the ssDNA-FQ reporters for RAVI-CRISPR assays. (A) Schematic diagram of the assay for determining ssDNA-FQ reporter activity based on exonuclease I cleavage (left) and subsequent evaluation under the blue or UV light or by the naked eye observation of colorimetric changes in the reaction solution (right). (B) Visual and end-point imaging evaluation of the excitation or colorimetric characteristics of 16 candidate ssDNA-FQ reporters after exonuclease I cleavage, 15 min incubation, and thermal denaturation. + represents a reaction with exonuclease I, − represents a reaction without exonuclease I. (C) Optimization of ssDNA-FQ reporter concentrations in RAVI-CRISPR assays. A fluorescence microplate reader was used to quantify the fluorescence intensity and background signals for individual ssDNA-FQ

**Figure** 1. continued

reporters at four concentrations (50 nM, 800 nM, 2.5 $\mu$M, and 30 $\mu$M), both before and after exonuclease I cleavage. Data are represented as means ± SEM; $n$ = 3. The images were captured under the blue (470 nM) or UV lights using a smartphone camera or the gel imaging system. The images were also captured under no excitation light using a smartphone camera.

used to locate and segment the images of the PCR tube tip to maximize the utilization of effective information of the images under no excitation light.

**2.9. Construction of a Binary Classification Model for Positive and Negative Detection Signals.** A CNN-based model was constructed for the binary classification of positive and negative detection signals. This CNN model was trained based on the TensorFlow (v1.13.1) and Keras (v2.1.5) frameworks and followed the procedures of François Chollet's suggestion in Deep Learning with Python to regularize the model and to optimize the hyperparameters as our previous research.[53,54] The CNN model consisted of four convolutional layers with 2D ConvNets, four pooling layers, and two fully connected layers. The "filter" parameters for convolutional layers were 32, 64, 128, and 128, and the remaining parameters were set as "kernel_size = (3,3), activation = relu". The parameters for pooling layers were set as "pool_size = (2,2)". For fully connected layers, after 512-way rectified linear unit (ReLU) layers, a one-way sigmoid layer was designed to return a probability score. Additionally, we exposed the model to multiple aspects of the images through data augmentation, such as image rotation, image shift, and image shear, to enhance the generalization power. The parameters were as follows: "rescale = 1./255, rotation_range = 40, width_shift_range = 0.2, height_shift_range = 0.2, shear_range = 0.2, zoom_range = 0.2, horizontal_flip = True". In addition, the MagicEye mobile phone app (Android version 1.0) was developed and can be freely downloaded from https://sourceforge.net/projects/ravi-crispr/files/MagicEye_en_v1.0.apk/download.

**2.10. Statistical Analysis.** Statistical analysis was performed using the R programming language. The mean ± standard error of the mean (SEM) was determined for each treatment group in separate experiments. The two-tailed Student's $t$ test was applied to determine significant differences between the treatment and control groups (\*\*\*$P$ < 0.001, ns: not significant at the 95% confidence level).

# 3. RESULTS

**3.1. Establishment of the Colorimetric RAVI-CRISPR Assay.** To identify the best reporter for the colorimetric RAVI-CRISPR assay, we screened a total of 16 types of ssDNA-FQ reporters using an exonuclease I digestion and subsequently optimized their concentrations for direct application in RAVI-CRISPR assays. The two main steps in the assay consisted of an exonuclease I digestion and a reporter signal read-out (Figure 1A). The colors emitted by different types of degraded ssDNA-FQ reporters in the reaction solution were then compared under a blue or UV light transilluminator, as well as with direct assessment by the naked eye using no excitation light. In addition, the fluorescence signal intensities of the intact or degraded ssDNA-FQ reporters were measured using a fluorescence microplate reader to establish background signals. The results showed that 14 of the degraded ssDNA-FQ reporters can emit strong fluorescence signals under the UV light transilluminator (Figure 1B).

Interestingly, we observed by the naked eye that more than nine of the degraded ssDNA-FQ reporters changed the color of the reaction solution in the PCR test tube without excitation light (Figure 1B and Table S2). For instance, the degraded ROX- or Texas RED-labeled reporter reactions exhibited obvious color changes from blue to red (Figure 1B). However, the degraded Cy5- and Cy5.5-labeled reporters were only found to emit fluorescence signals under UV light, while the degraded Cy7-labeled reporter did not emit any fluorescent signal nor change the color in reaction solutions (Figure 1B). In conclusion, these results indicated that some ssDNA-FQ reporter modifications had better optical properties than others.

In the naked-eye detection of nucleic acids, the optimal concentrations of ssDNA-FQ reporters significantly improved the visual colorimetry (Figure S1A−P). However, for enhanced fluorescence visualization assays, background noise was concurrently increased with increasing signals for VIC-, TET-, and FAM-labeled reporters, resulting in potential interference with detection accuracy (Figure S1A−P). In Figure 1C, using a fluorescence microplate reader, the excessive background fluorescence signals of 16 ssDNA-FQ reporters have been detected in different concentrations, and the corresponding signal-to-noise (*e.g.*, background fluorescence signals) ratio was also calculated (Table S3). We found that for VIC-, TET-, or FAM-labeled ssDNA-FQ reporters, higher concentrations resulted in excessive background fluorescence signals (Figure 1C and Table S3). As expected, the signal-to-noise ratio of the ROX-dye ssDNA-FQ reporter was relatively higher than other reporters at the same concentration, and its ratio can be increased with the increase of reporter concentration, indicating that this type of modification had the lowest background fluorescent signal and therefore suitable for the CRISPR-based detection assay (Table S3).

Taken together, we suggested that an optimal concentration should be determined and adjusted for each ssDNA-FQ reporter type depending on the method used to assess the read-out by either fluorescence excitation or the naked-eye evaluation with no excitation light. For instance, for a more accurate colorimetric naked-eye detection, the optimal concentration was the ROX-labeled reporter at ≥5 $\mu$M (Figure S1A). However, for the detection of fluorescence intensity under a blue light transilluminator, the minimal concentration of ROX-labeled reporter was 100 nM after 15 min of incubation to obtain a full saturation (Figure S1A). Given the strong performance of the ROX dye, we selected the ROX-labeled reporters for all subsequent experiments.

**3.2. SARS-CoV-2 Detection by the RAVI-CRISPR Assay.** To develop a highly sensitive diagnostics for the nucleic acids of SARS-CoV-2 using the RAVI-CRISPR system and the naked-eye detection, five crRNAs for the SARS-CoV-2 E gene (E-crRNA-1 to 5) and nine crRNAs for the SARS-CoV-2 N gene (N-crRNA-1 to 9) were screened for their efficiency of target cleavage (Figure S2A). First, we compared the activities of these crRNAs using PCR products and the corresponding ssDNA activators as templates. The results
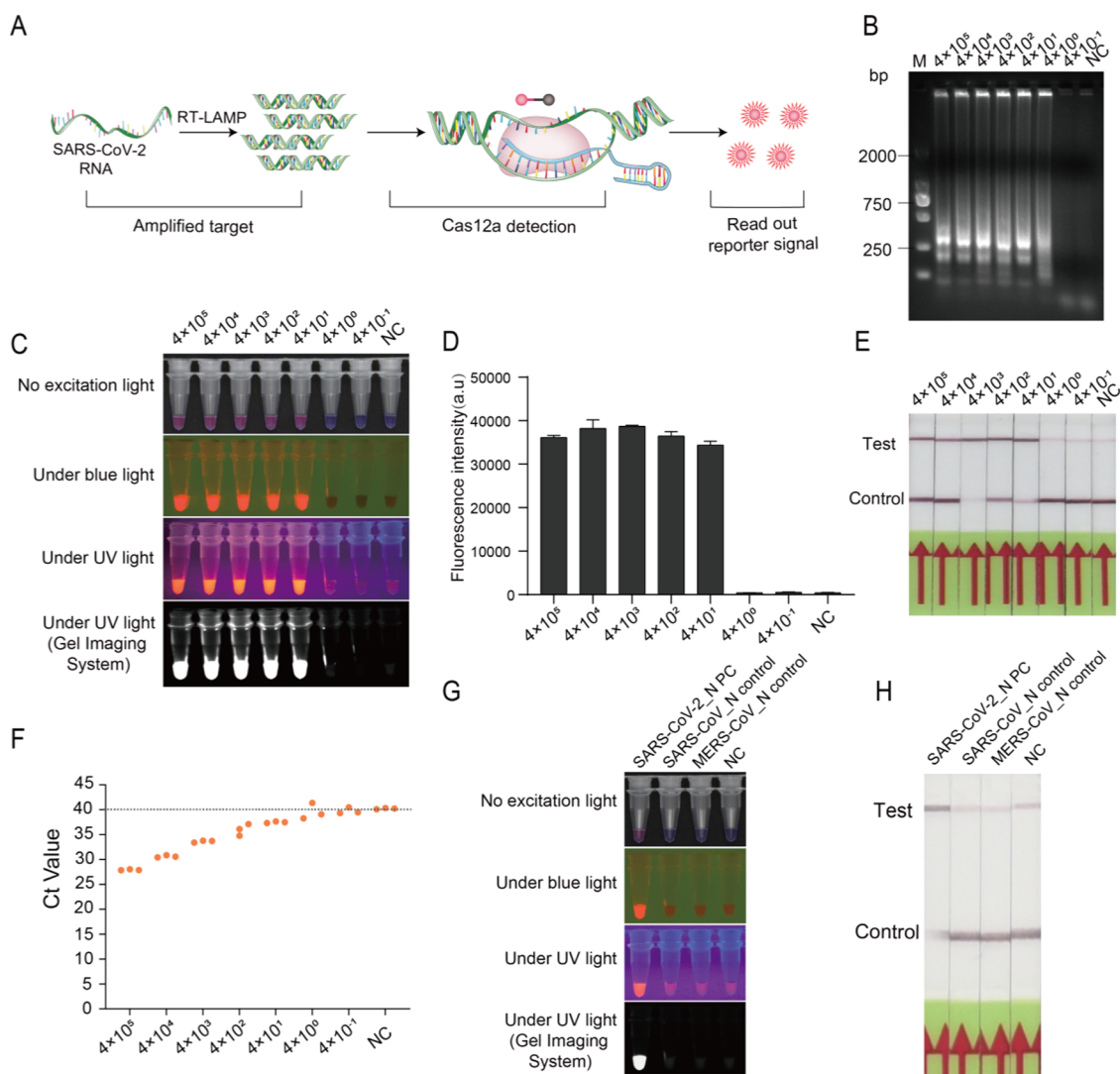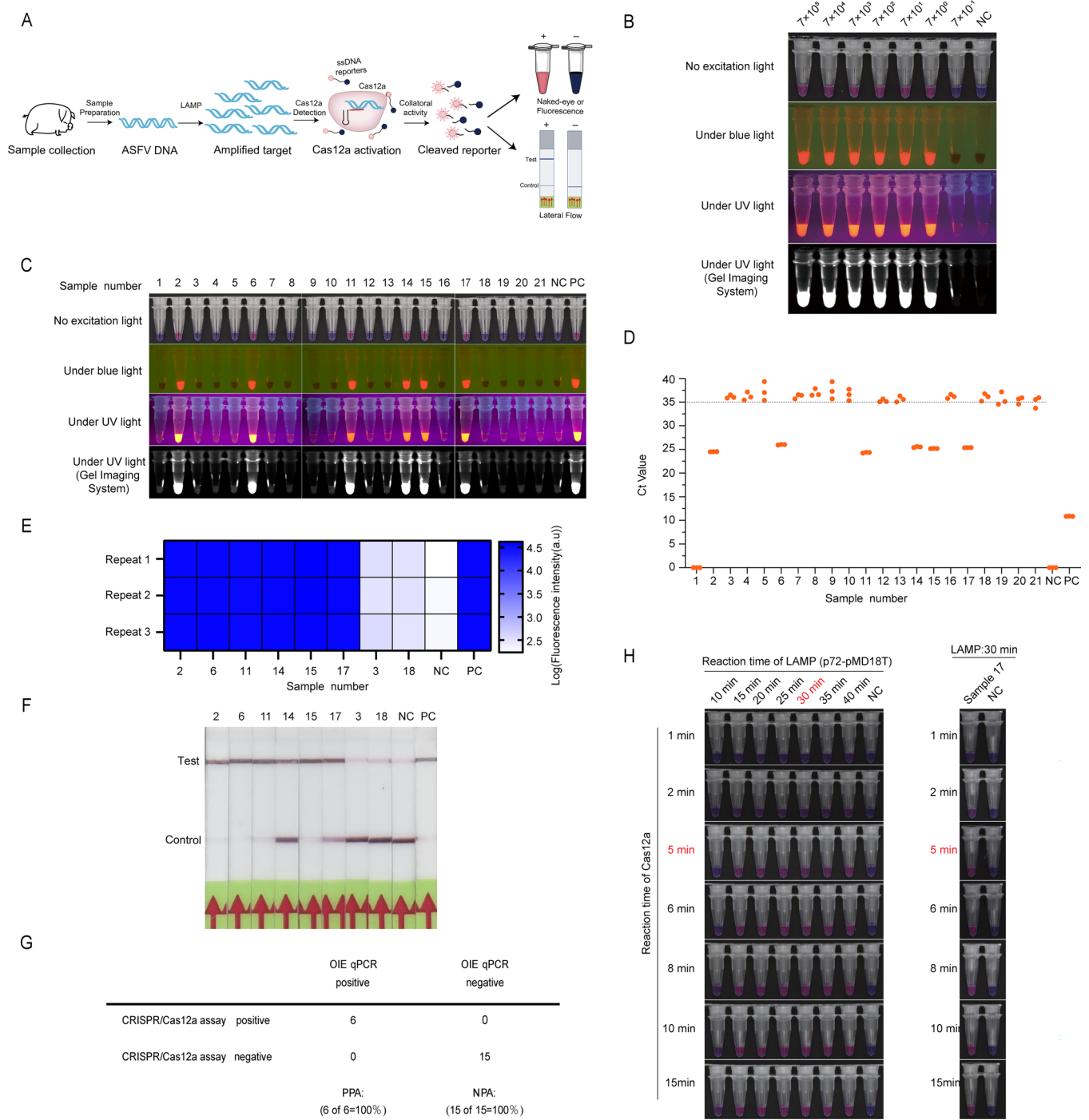
**Figure 2.** Sensitivity and specificity of the RAVI-CRISPR assay for the detection of *in vitro* SARS-CoV-2 *N* gene transcripts. (A) Schematic diagram of the RAVI-CRISPR assay for the detection of SARS-CoV-2. (B) Agarose gel electrophoresis determination of the limit of detection for RT-LAMP amplification of the SARS-CoV-2 *N* gene. (C) Colorimetric signal detection of a 10-fold serial dilution of *in vitro* SARS-CoV-2 *N* gene transcripts using the RAVI-CRISPR assay. (D) Sensitivity of the RAVI-CRISPR assay quantified with a multifunctional microplate reader. (E) Sensitivity of the RAVI-CRISPR-based lateral flow strip assay. (F) Sensitivity of the detection of *in vitro* SARS-CoV-2 *N* gene transcripts by RT-qPCR using a CFX96 Touch Real-Time PCR Detection System. (G) Specificity of the RAVI-CRISPR assay evaluated by the naked eye or fluorescent visual detection. (H) Specificity of the RAVI-CRISPR-based lateral flow strip assay. Data are represented as means ± SEM; *n* = 3. NC stands for negative control, while PC stands for positive control.

showed that E-crRNA-2 and E-crRNA-5 exhibited the highest activity for the detection of the *E* gene (Figure S2B), while N-crRNA-5, N-crRNA-6, N-crRNA-7, and N-crRNA-9 showed sufficient activity for the detection of the *N* gene (Figure S2C). Subsequent experiments used only E-crRNA-5 and N-crRNA-9 for the detection of SARS-CoV-2.

To further evaluate the sensitivity of the RAVI-CRISPR technology for SARS-CoV-2 detection, *in vitro*-transcribed RNAs of the *N* and *E* genes from two synthetic plasmids, each carrying one of the target genes, were used as a template (Figure 2A). Following a concentration gradient, we determined that the limit of detection (LoD) for amplification by the RT-LAMP assay was 40 total copies (Figure 2B). Subsequently, the amplified product of the RT-LAMP *N* gene was digested by Cas12a and subjected to detection. The result showed that the sensitivity of this technique also reached 40 total copies, implying that the limiting step was the RT-LAMP

reaction (Figure 2C). The fluorescence signal intensity of the RAVI-CRISPR assay was further measured using a fluorescence microplate reader (Figure 2D), which confirmed the detection by the naked eye with or without excitation light. In addition, we tested both a lateral-flow paper strip assay integrated with CRISPR/Cas12a (Figure 2E) as well as a traditional RT-qPCR assay (Figure 2F); the results of both assays were consistent with the sensitivity of the direct naked-eye detection without excitation light. For example, we observed that RT-qPCR Ct values were ≥40 for sample concentrations ≤4 total copies (Figure 2F and Table S4), which can be considered as negative results. Furthermore, we found that the RAVI-CRISPR technology can directly detect the *N* gene of SARS-CoV-2 by the naked eye assessment but cannot detect its orthologue *N* gene of SARS-CoV or MERS-CoV (Figure 2G). This specificity was consistent with the

**Figure 3.** Sensitivity and specificity of the RAVI-CRISPR assay for the detection of ASFV in clinical samples. (A) Schematic diagram of steps in the RAVI-CRISPR assay for the detection of ASFV. (B) Sensitivity of the RAVI-CRISPR assay determined using 10-fold serial dilutions of ASFV p72 plasmid DNA. (C) Naked eye detection of ASFV in blood samples by the RAVI-CRISPR assay under blue, UV, or no excitation light conditions. (D) Detection of ASFV in blood samples by qPCR ($n = 21$) using a CFX96 Touch Real-Time PCR Detection System. (E) Microplate reader quantification of selected ASFV in blood samples confirmed by the RAVI-CRISPR assay. (F) RAVI-CRISPR-based lateral flow strip assay detection of selected ASFV in blood samples confirmed by the RAVI-CRISPR assay. (G) Comparison of the detection results of selected ASFV in blood samples by the RAVI-CRISPR-based and OIE qPCR-based assays. PPA stands for positive predictive agreement, while NPA stands for negative predictive agreement. (H) Evaluation of different reaction incubation times for LAMP amplification and CRISPR cleavage for the RAVI-CRISPR assay. NC stands for negative control, while PC stands for positive control.

SARS-CoV-2 $N$ gene detected by CRISPR/Cas12a combined with a lateral-flow paper strip (Figure 2H).

We next examined the sensitivity and specificity of SARS-CoV-2 $E$ gene detection by the RAVI-CRISPR assay. Using the concentration gradient, we determined the LoD for RT-LAMP

amplification of the SARS-CoV-2 $E$ gene to be 58 total copies (Figure S3A). The amplified product of the $E$ gene was then digested by Cas12a for naked-eye detection under different light conditions. The result showed that the sensitivity of this technique reached 58 total copies (Figure S3B), which was

G
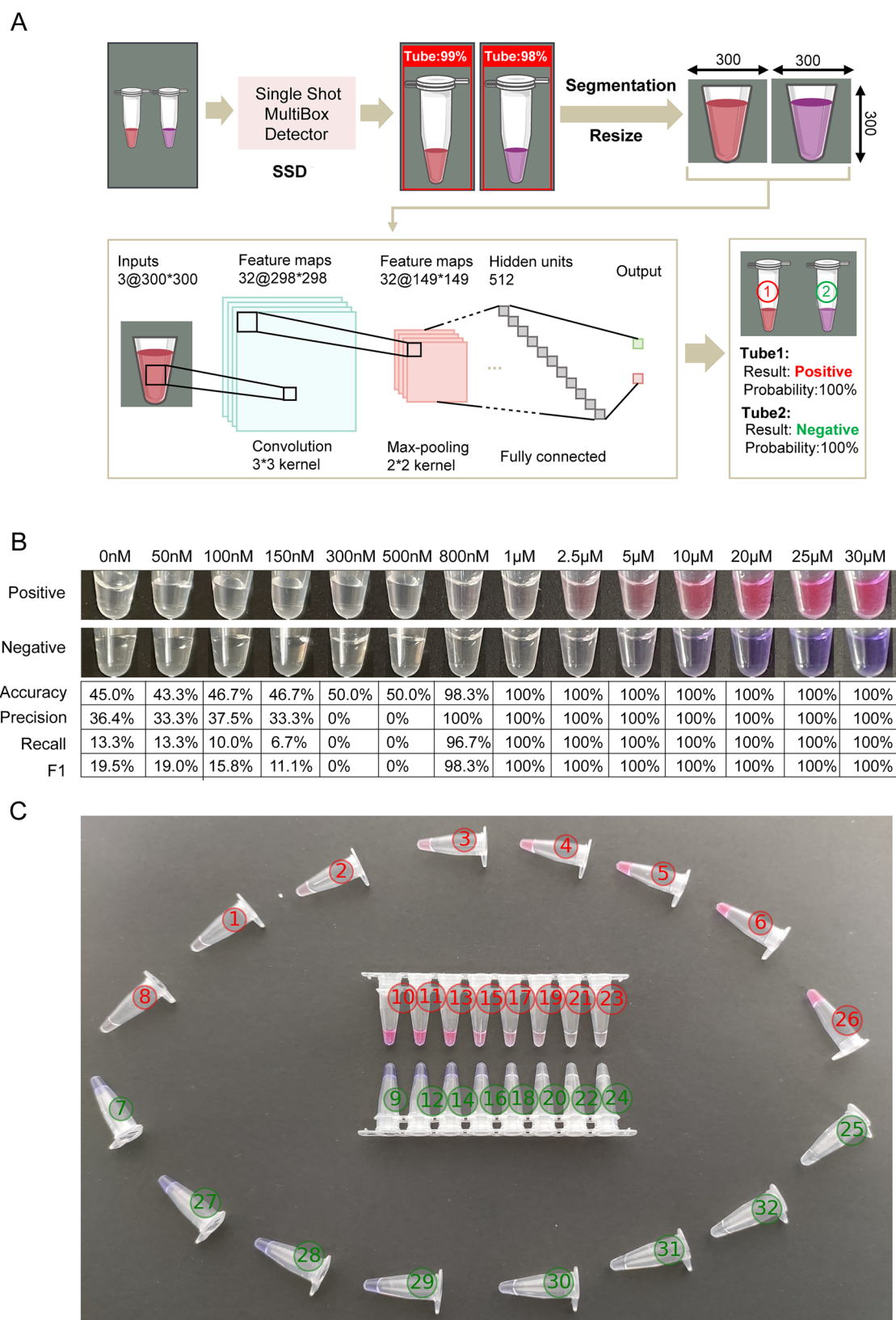
**Figure 4.** Analysis of the RAVI-CRISPR assay read-outs by two convolutional neural network-based machine learning models. (A) Single Shot MultiBox Detector (SSD) algorithm identification of reaction tubes and binary classification of positive or negative detection signals. (B) Performance of the binary classification model for nucleic acid detection under different ROX-labeled reporter concentrations. F1 stands for F1-measure, which was used to evaluate the accuracy of predictions in two-class (binary) classification problems. (C) Demonstration of the binary classification model for nucleic acid detection. Red font indicates that the corresponding PCR tube was classified as positive, whereas green indicates its classification as negative.

H
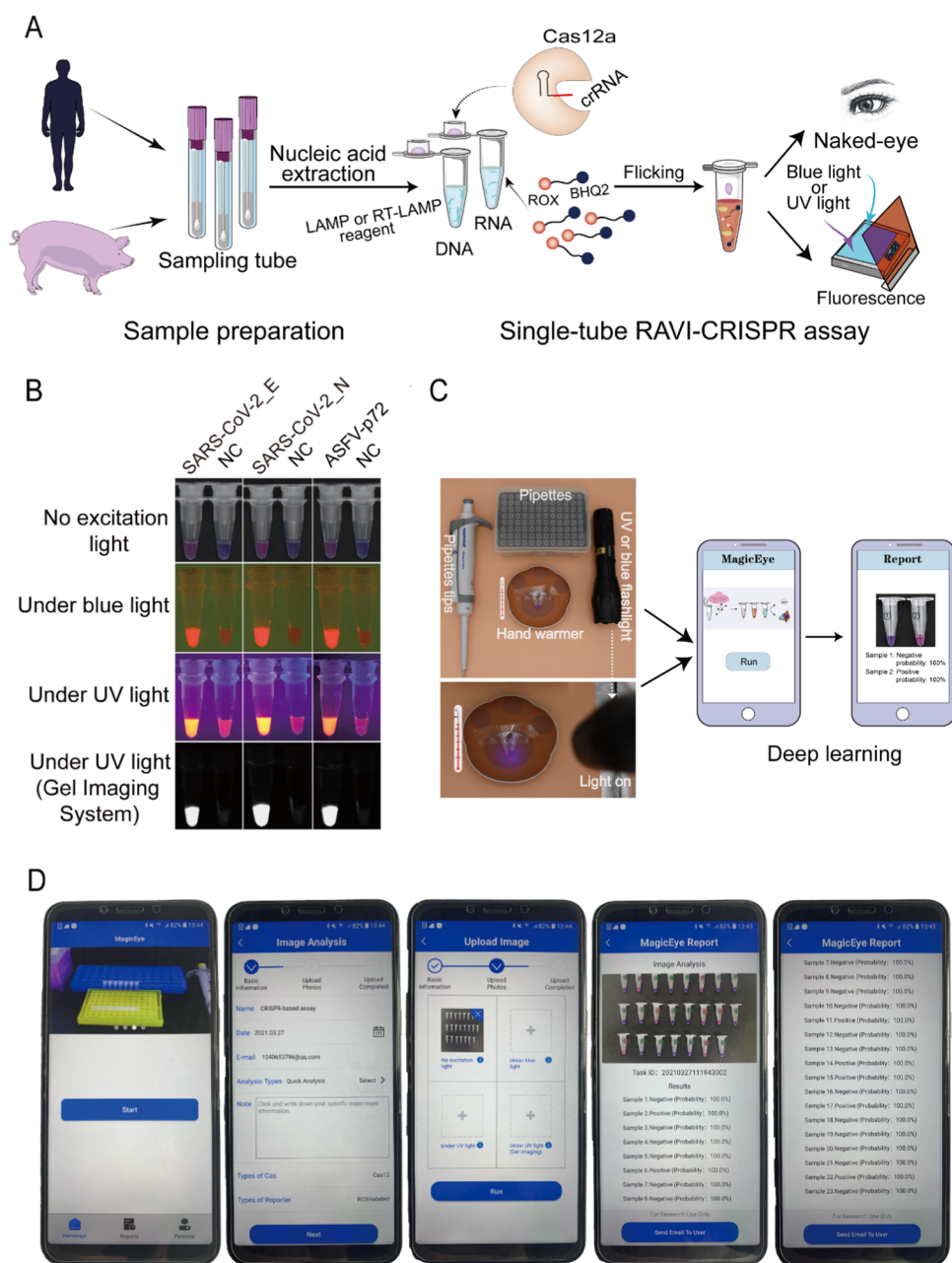
**Figure 5.** Establishment of the contamination-free single-tube RAVI-CRISPR assay and mobile MagicEye system for the point-of-care detection of nucleic acids. (A) Diagram of the overall experimental flow and principle of the contamination-free single tube RAVI-CRISPR assay. (B) Visual detection of the SARS-CoV-2 E and N genes as well as the ASFV *p72* gene by the single-tube RAVI-CRISPR assay. (C) Photo display of portable rechargeable hand warmers and smartphones for point-of-care testing. (D) Diagram of the analytical results for 21 clinical samples suspected of ASFV infection by the MagicEye app.

confirmed by microplate reading (Figure S3C). As with the *N* gene, both CRISPR/Cas12a combined with lateral-flow paper strip (Figure S3D) and traditional RT-qPCR assays (Figure S3E and Table S4) showed comparable sensitivity for the detection of SARS-CoV-2 *E* gene with that of the RAVI-CRISPR assay. Specifically, the Ct values observed in the RT-qPCR assay at the sample concentration ≤5.8 total copies were ≥40 (Figure S3E and Table S4), indicating a negative result. These results confirmed the sensitivity of this technique to be 58 total copies for the SARS-CoV-2 *E* gene. Finally, we found that the RAVI-CRISPR system has high specificity for detecting the SARS-CoV-2 *E* gene, and it can clearly distinguish the targeted *E* gene from different SARS family

viruses (Figure S3F). This result was further confirmed with the CRISPR/Cas12a−lateral flow paper strip combination assay (Figure S3G). Thus, the RAVI-CRISPR systems using RT-LAMP coupled with CRISPR/Cas12a allowed a robust detection of the SARS-CoV-2 *E* and *N* genes with high sensitivity and specificity.

**3.3. ASFV Detection by the RAVI-CRISPR Assay.** Considering our result showing effective detection of SARS-CoV-2, we next developed a fast, sensitive, and reliable RAVI-CRISPR-based assay for ASFV using a highly active crRNA identified in our previous study.[37] The strategy for ASFV detection was similar to that for SARS-CoV-2 except that a standard LAMP for DNA amplification was used rather than

RT-LAMP since ASFV is a DNA virus (Figure 3A). We first evaluated the sensitivity of ASFV *p72* gene by RAVI-CRISPR visual detection using a concentration gradient to determine the LoD to be seven total copies (Figure 3B and Table S5). Subsequently, we assessed our system using 21 clinical samples previously diagnosed using a qPCR recommended by the World Organisation for Animal Health (OIE). The result showed 100% consistency between the naked eye assessment of RAVI-CRISPR-based assay under different light conditions (Figure 3C) and the qPCR result (Figure 3D) for both ASFV negative and positive samples. Notably, the negative samples with Ct values observed in the OIE qPCR ≥35 were confirmed by the RAVI-CRISPR assay (Table S6).

Moreover, the read-outs of the RAVI-CRISPR assay were further validated using a multifunctional microplate reader (Figure 3E) and the CRISPR/Cas12a-integrated lateral-flow paper strip assay (Figure 3F). All of these results indicated that the detection of ASFV *p72* gene using the CRISPR/Cas12a-based assay can be accurately applied in the clinical screening of ASF samples (Figure 3G). In addition, we evaluated the optimal reaction time for RAVI-CRISPR read-out using a *p72* gene-containing plasmid as the template. The result showed that the shortest reaction time necessary for the LAMP reaction to reach saturation was around 30 min, while the minimum reaction time required for Cas12a cleavage in the naked-eye detection was around 5 min (Figure 3H). Therefore, this optimized RAVI-CRISPR assay including only 35 min of incubation can detect as few as seven total copies of viral gene per reaction, which was further verified by the screening of clinical samples suspected of ASFV infection (Figure 3H).

### 3.4. Convolutional Neural Network Assessment of the Read-Out of the RAVI-CRISPR Assay.

To provide the RAVI-CRISPR assay as a convenient package including a standardized evaluation mode, we developed the MagicEye mobile phone app that employed two machine learning models based on CNN to automatically interpret the results of nucleic acids detection in multiple reaction tubes (Figure 4A). The first model was for object detection, which used a Single Shot MultiBox Detector (SSD) algorithm to identify the images of reaction tubes.[50] The second model was for binary classification of either positive or negative signals to resolve the operator-associated inconsistencies across the naked-eye detection.

To train the first model to recognize the images of PCR tubes, we used 1554 single-PCR tube images, 405 multiple PCR tube images, 283 eight-tube PCR strip images, and 301 mixed images (eight-tube PCR strip mixed with single-PCR tube images) that were manually labeled (Table S7). Testing of the object detection model showed that this algorithm could identify PCR tubes in all cases (Figure S4) with the detection rates at 100% for both single and multiple PCR tube images and >99% for eight-tube PCR strip images (Table S8). Subsequently, the binary classification model was trained to distinguish colorimetric changes in the tubes containing the RAVI-CRISPR reactions with either positive or negative detection signals (Table S9). We found that the F1-measure, which was used to evaluate the accuracy of predictions in two-class (binary) classification problems, could be increased to 100% using an optimal ROX-labeled reporter in concentration >1 $\mu$M (Figure 4B). This result meant that the model performed well on images captured with no excitation light when the probe concentration was relatively high (Figure 4C).

To evaluate the robustness of the model at critical concentrations of DNA samples, using images captured under no excitation light as an example, we tested the model on samples with probe concentrations of 1 $\mu$M and DNA concentrations ranging from 0 to $7 \times 10^5$ total copies. The result showed that even at a very low concentration of the DNA template, the model could discriminate negative and positive signals with 100% accuracy (Figure S5 and Table S10). We also found that the sensitivity of the image analysis app was much higher than that of the naked eye read-out, indicating that the power of the app can be used in circumstances where higher throughput testing of clinical/agricultural samples for small—mid-sized farms or accessibility for the visually impaired.

To further evaluate the classification model, we examined the ConvNet outputs at the intermediate training stage of the convolutional model and found that many activation channels were focused on the tip of the PCR tube (Figure S6), suggesting that the model may classify results primarily by distinguishing the tip color where the signal was the strongest, in the same way as the naked-eye observation. Finally, we deployed this algorithm on a cloud server as the MagicEye mobile application for accurate and rapid analysis of nucleic acid detection signals.

### 3.5. Single-Tube RAVI-CRISPR Assay and Mobile MagicEye System for POCT of Nucleic Acids.

The two-step RAVI-CRISPR assay requires opening of the tube after the RT-LAMP or LAMP reaction, which may generate aerosols, potentially causing false-positive results. To reduce the likelihood of contamination and improve the convenience of the visualization process for POCT of SARS-CoV-2 or ASFV, we next established a single-tube RAVI-CRISPR assay. The underlying principle and operation of the assay relied on an isothermal amplification with CRISPR/Cas12a-based detection (Figure 5A). To avoid cross-contamination, mineral oil was added to cover the extracted nucleic acids and isothermal amplification solution. Cas12a and crRNA ribonucleoproteins (RNPs) reagents were pre-added inside of the tube lid. Following the isothermal amplification, RNP reagents were mixed with amplification reagents by flicking (Figure 5A). The whole process did not require the lid to be reopened, thus avoiding the possibility of aerosol contamination.

Next, we tested the combined single-tube RAVI-CRISPR/MagicEye system with simulated *in vitro* transcripts or real clinical samples and found that the SARS-CoV-2 *E* and *N* genes and the ASFV *p72* genes were all successfully detected (Figure 5B). To facilitate the pen- or bed-side, instrument-less detection of virus, we used a portable rechargeable hand warmer to provide temperatures from 35 to 60 °C for the amplification incubation. To enhance the fluorescence signal for the pen- or bed-side detection, a small flashlight capable of UV and blue light emission was approved to be sufficient (Figure 5C). Analysis using a smartphone with the MagicEye app successfully replicated the result of detection by the naked eye for these samples (Figures 5D and S7 and Table S11), thereby demonstrating this single-tube RAVI-CRISPR assay, instrumented only with a portable rechargeable hand warmer and MagicEye app, to be readily deployable as pen- or bed-side POCT of SARS-CoV-2 or ASFV among other viral pathogens.

## 4. DISCUSSION

Current and future global pandemics of viral infections, like the ongoing COVID-19 pandemic caused by SARS-CoV-2, pose

overwhelming threats to human health and global economic stability. Thus, the development of affordable and convenient POCT diagnostic tools is both warranted and urgent. In the present study, we have developed a rapid, single-tube, instrument-less, colorimetric POCT assay ("RAVI-CRISPR") for the detection of nucleic acids as a demonstration of the proof-of-concept for its sensitive detection of diverse pathogenic nucleic acids by the naked eye. Particularly, we developed the MagicEye mobile app for standardized diagnostic image analysis of color changes in the reaction tubes. The main feature of this POCT assay is that ssDNA-FQ reporters are used as colorimetric sensors to produce changes in the color of the reaction mixture dependent on the concentrations of the reporters and specifically targeted nucleic acids that are cleaved by Cas12a. To our knowledge, this is the simplest CRISPR-based nucleic acid platform reported to date, since no fluorescence detector is required for visualization (Table S12).

Although previous studies have reported that the LAMP reaction can amplify targeted nucleic acids with high efficiency, this reaction produces long concatemeric amplicons, which make sequence-specific detection of LAMP products analytically challenging.[26] A recent study reported that the use of CRISPR/Cas12a in combination with a sequence-specific plasmonic LAMP assay can provide orthogonal color read-outs.[55] However, plasmonic gold nanoparticles (AuNPs) are difficult to produce and their waste is hard to manage, thus limiting their application. To resolve these issues, ssDNA-FQ reporters are proven to be straightforward to synthesize and environmentally harmless compared to AuNPs. We found that the ssDNA-FQ reporter concentration exerts a strong impact on the direct visual detection of nucleic acids. By adjusting the concentration of the ROX-labeled reporter, clear naked-eye observation of the detected nucleic acids became feasible without excitation light. In comparison, colorimetric detection with our RAVI-CRISPR system using the ROX-labeled reporter produced stronger color changes than that of the AIOD-CRISPR assay, which used FAM-labeled reporters.[41] In particular, our optimization process identified eight ssDNA-FQ reporters suitable for direct assessment with no excitation light. In addition, we found that the control bands in several of the lateral flow assays are light or absent (Figure 2E,F). Our result was almost consistent with that found by other studies, which showed that the control band was not present when there was complete digestion of the reporter molecule by Cas12.[34]

To facilitate the standardization for colorimetric image detection, we also developed a cloud server-based, CNN algorithm (MagicEye app) for automatic analysis of the testing results. Although two apps, HandLens[43] and STOPCovid.v2,[44] were previously developed for CRISPR-based nucleic acid detection, these apps only focused on image analysis of lateral flow strip read-outs, whereas MagicEye can recognize and analyze colorimetric changes of single or eight-strip PCR tubes in multiple test reactions (Table S12). Our MagicEye can also improve the detection sensitivity of RAVI-CRISPR assays. The accurate diagnosis of ASFV infection in pigs by MagicEye and visual inspection confirmed the reliability of the RAVI-CRISPR assay. This assay was successfully used for the highly sensitive detection of ASFV samples in a single-tube incubated only by a portable rechargeable hand warmer. In addition, the MagicEye app can be used for higher throughput testing of clinical/agricultural samples for small—mid-sized farms or accessibility for the visually impaired. Moreover, this system does not require an electrical power source; therefore, it can be feasibly deployed for pen- or bed-side testing in rural areas with limited resources.

To sum up, we report the establishment of a low-cost (∼U.S. $1), highly sensitive, single-tube method for colorimetric, naked-eye detection of nucleic acids based on CRISPR/Cas12a, with an accompanying cloud-based CNN app for standardized, multisample diagnostic analyses. We screened ssDNA-FQ reporters and optimized their concentrations for colorimetric detection of viral nucleic acids. We then developed the RAVI-CRISPR assay using LAMP amplification and CRISPR-Cas12a cleavage as a single-tube, instrument-less reaction. In particular, we developed the MagicEye mobile application for standardized evaluation of nucleic acid detection read-outs, which uses a CNN algorithm to accurately and rapidly analyze results. The low-cost, high sensitivity, and high specificity of the RAVI-CRISPR/MagicEye system can enable rapid, on-site detection of SARS-CoV-2 or ASFV, or can be modified for other pathogens by an automated analysis.

## ■ ASSOCIATED CONTENT

### ⓢ Supporting Information

The Supporting Information is available free of charge at https://pubs.acs.org/doi/10.1021/acssynbio.1c00474.

> Detection ability of 16 ssDNA-FQ reporters under different concentrations; selection of highly active crRNAs for detection of SARS-CoV-2 *E* and *N* genes; the sensitivity and specificity of RAVI-CRISPR for the detection of *in vitro* SARS-CoV-2 *E* gene transcripts; demonstration of the PCR tube image object detection model; sensitivity of the binary classification model for nucleic acid detection; visualization of all activation layers in the PCR tube image; analysis of RAVI-CRISPR read-outs for ASFV in clinical samples; the signal-to-noise ratio of the cleaved ssDNA-FQ reporters under different concentrations; the discernible and optimal range of concentrations for different ssDNA-FQ reporters under different light conditions; standard curves of OIE, CDC, and WHO qRT-PCR assays; comparison of the accuracy of RAVI-CRISPR and qPCR technology in detecting ASFV in clinical samples; and tables of oligo sequences and sgRNAs used in the study (PDF)

## ■ AUTHOR INFORMATION

### Corresponding Authors

**Xinyun Li** — *Key Laboratory of Agricultural Animal Genetics, Breeding and Reproduction of Ministry of Education & Key Lab of Swine Genetics and Breeding of Ministry of Agriculture and Rural Affairs, Huazhong Agricultural University, Wuhan 430070, P. R. China; The Cooperative Innovation Center for Sustainable Pig Production, Huazhong Agricultural University, Wuhan 430070, P. R. China; Hubei Hongshan Laboratory, Frontiers Science Center for Animal Breeding and Sustainable Production, Wuhan 430070, P. R. China*; Email: xyli@mail.hzau.edu.cn

**Xiaolei Liu** — *Key Laboratory of Agricultural Animal Genetics, Breeding and Reproduction of Ministry of Education & Key Lab of Swine Genetics and Breeding of Ministry of Agriculture and Rural Affairs, Huazhong Agricultural University, Wuhan 430070, P. R. China; The Cooperative*

*Innovation Center for Sustainable Pig Production, Huazhong Agricultural University, Wuhan 430070, P. R. China; Hubei Hongshan Laboratory, Frontiers Science Center for Animal Breeding and Sustainable Production, Wuhan 430070, P. R. China;* Email: xiaoleiliu@mail.hzau.edu.cn

**Shuhong Zhao** − *Key Laboratory of Agricultural Animal Genetics, Breeding and Reproduction of Ministry of Education & Key Lab of Swine Genetics and Breeding of Ministry of Agriculture and Rural Affairs, Huazhong Agricultural University, Wuhan 430070, P. R. China; The Cooperative Innovation Center for Sustainable Pig Production, Huazhong Agricultural University, Wuhan 430070, P. R. China; Hubei Hongshan Laboratory, Frontiers Science Center for Animal Breeding and Sustainable Production, Wuhan 430070, P. R. China;* Email: shzhao@mail.hzau.edu.cn

## Authors

**Shengsong Xie** − *Key Laboratory of Agricultural Animal Genetics, Breeding and Reproduction of Ministry of Education & Key Lab of Swine Genetics and Breeding of Ministry of Agriculture and Rural Affairs, Huazhong Agricultural University, Wuhan 430070, P. R. China; Animal and Human Health Program, Biosciences, International Livestock Research Institute (ILRI), Nairobi 00100, Kenya; The Cooperative Innovation Center for Sustainable Pig Production, Huazhong Agricultural University, Wuhan 430070, P. R. China;* orcid.org/0000-0002-8301-877X

**Dagang Tao** − *Key Laboratory of Agricultural Animal Genetics, Breeding and Reproduction of Ministry of Education & Key Lab of Swine Genetics and Breeding of Ministry of Agriculture and Rural Affairs, Huazhong Agricultural University, Wuhan 430070, P. R. China*

**Yuhua Fu** − *Key Laboratory of Agricultural Animal Genetics, Breeding and Reproduction of Ministry of Education & Key Lab of Swine Genetics and Breeding of Ministry of Agriculture and Rural Affairs, Huazhong Agricultural University, Wuhan 430070, P. R. China*

**Bingrong Xu** − *Key Laboratory of Agricultural Animal Genetics, Breeding and Reproduction of Ministry of Education & Key Lab of Swine Genetics and Breeding of Ministry of Agriculture and Rural Affairs, Huazhong Agricultural University, Wuhan 430070, P. R. China*

**You Tang** − *Electrical and Information Engineering College, Jilin Agricultural Science and Technology University, Jilin 132101, P. R. China*

**Lucilla Steinaa** − *Animal and Human Health Program, Biosciences, International Livestock Research Institute (ILRI), Nairobi 00100, Kenya*

**Johanneke D. Hemmink** − *Animal and Human Health Program, Biosciences, International Livestock Research Institute (ILRI), Nairobi 00100, Kenya*

**Wenya Pan** − *Key Laboratory of Agricultural Animal Genetics, Breeding and Reproduction of Ministry of Education & Key Lab of Swine Genetics and Breeding of Ministry of Agriculture and Rural Affairs, Huazhong Agricultural University, Wuhan 430070, P. R. China*

**Xin Huang** − *Key Laboratory of Agricultural Animal Genetics, Breeding and Reproduction of Ministry of Education & Key Lab of Swine Genetics and Breeding of Ministry of Agriculture and Rural Affairs, Huazhong Agricultural University, Wuhan 430070, P. R. China*

**Xiongwei Nie** − *Key Laboratory of Agricultural Animal Genetics, Breeding and Reproduction of Ministry of Education*

& *Key Lab of Swine Genetics and Breeding of Ministry of Agriculture and Rural Affairs, Huazhong Agricultural University, Wuhan 430070, P. R. China*

**Changzhi Zhao** − *Key Laboratory of Agricultural Animal Genetics, Breeding and Reproduction of Ministry of Education & Key Lab of Swine Genetics and Breeding of Ministry of Agriculture and Rural Affairs, Huazhong Agricultural University, Wuhan 430070, P. R. China*

**Jinxue Ruan** − *Key Laboratory of Agricultural Animal Genetics, Breeding and Reproduction of Ministry of Education & Key Lab of Swine Genetics and Breeding of Ministry of Agriculture and Rural Affairs, Huazhong Agricultural University, Wuhan 430070, P. R. China*

**Yi Zhang** − *Key Laboratory of Agricultural Animal Genetics, Breeding and Reproduction of Ministry of Education & Key Lab of Swine Genetics and Breeding of Ministry of Agriculture and Rural Affairs, Huazhong Agricultural University, Wuhan 430070, P. R. China*

**Jianlin Han** − *CAAS-ILRI Joint Laboratory on Livestock and Forage Genetic Resources, Institute of Animal Science, Chinese Academy of Agricultural Sciences (CAAS), Beijing 100193, P. R. China; LiveGene Program, Biosciences, International Livestock Research Institute (ILRI), Nairobi 00100, Kenya*

**Liangliang Fu** − *Key Laboratory of Agricultural Animal Genetics, Breeding and Reproduction of Ministry of Education & Key Lab of Swine Genetics and Breeding of Ministry of Agriculture and Rural Affairs, Huazhong Agricultural University, Wuhan 430070, P. R. China*

**Yunlong Ma** − *Key Laboratory of Agricultural Animal Genetics, Breeding and Reproduction of Ministry of Education & Key Lab of Swine Genetics and Breeding of Ministry of Agriculture and Rural Affairs, Huazhong Agricultural University, Wuhan 430070, P. R. China*

Complete contact information is available at:
https://pubs.acs.org/10.1021/acssynbio.1c00474

## Author Contributions

○S.X., D.T., Y.F., and B.X. contributed equally to this work. Most of the experimental work and data analysis were co-conducted by D.T., B.X., and S.X., with minor contributions from W.P., X.H., C.Z., J.R., L.F., X.N., Y.Z., Y.M., L.S., and J.H. Y.F. developed CNN assessment of RAVI-CRISPR assay read-outs. Y.T. developed the MagicEye mobile application. S.X. conceived the project, designed the experiments, and wrote the manuscript. S.Z., X.L., and X.L. provided support and supervised the project. All authors contributed to manuscript revision.

## Notes

The authors declare no competing financial interest.

## ■ ABBREVIATIONS

CRISPR, clustered regularly interspaced short palindromic repeats; crRNA, CRISPR-derived RNA; ssDNA-FQ reporter, single-stranded DNA-fluorophore-quencher reporter; LAMP, loop-mediated isothermal amplification; SARS-CoV-2, severe acute respiratory syndrome coronavirus 2; ASFV, African swine fever virus; MERS-CoV, Middle East respiratory syndrome coronavirus; SARS-CoV, severe acute respiratory syndrome coronavirus; Ct, cycle threshold; ssDNA, single-stranded DNA; POCT, point-of-care testing; CNN, convolutional neural network; APPs, mobile phone applications

## ■ REFERENCES

(1) Yu, A. C.; et al. Nucleic acid-based diagnostics for infectious diseases in public health affairs. *Front. Med.* 2012, 6, 173−186.

(2) Ngo, H. T.; Gandra, N.; Fales, A. M.; Taylor, S. M.; Vo-Dinh, T. Sensitive DNA detection and SNP discrimination using ultrabright SERS nanorattles and magnetic beads for malaria diagnostics. *Biosens. Bioelectron.* 2016, 81, 8−14.

(3) Zhao, X.; Lin, C. W.; Wang, J.; Oh, D. H. Advances in rapid detection methods for foodborne pathogens. *J. Microbiol. Biotechnol.* 2014, 24, 297−312.

(4) Wang, C.; Horby, P. W.; Hayden, F. G.; Gao, G. F. A novel coronavirus outbreak of global health concern. *Lancet* 2020, 395, 470−473.

(5) Cheng, M. P.; et al. Diagnostic Testing for Severe Acute Respiratory Syndrome-Related Coronavirus 2: A Narrative Review. *Ann. Intern. Med.* 2020, 172, 726−734.

(6) Xu, M.; et al. COVID-19 diagnostic testing: Technology perspective. *Clin. Transl. Med.* 2020, 10, No. e158.

(7) Vandenberg, O.; Martiny, D.; Rochas, O.; van Belkum, A.; Kozlakidis, Z. Considerations for diagnostic COVID-19 tests. *Nat. Rev. Microbiol.* 2021, 19, 171−183.

(8) Guinat, C.; et al. Transmission routes of African swine fever virus to domestic pigs: current knowledge and future research directions. *Vet. Rec.* 2016, 178, 262−267.

(9) Galindo, I.; Alonso, C. African Swine Fever Virus: A Review. *Viruses* 2017, 9, 103.

(10) Probst, C.; et al. The potential role of scavengers in spreading African swine fever among wild boar. *Sci. Rep.* 2019, 9, No. 11450.

(11) Sánchez-Cordón, P. J.; Montoya, M.; Reis, A. L.; Dixon, L. K. African swine fever: A re-emerging viral disease threatening the global pig industry. *Vet. J.* 2018, 233, 41−48.

(12) Yang, S.; Rothman, R. E. PCR-based diagnostics for infectious diseases: uses, limitations, and future applications in acute-care settings. *Lancet Infect. Dis.* 2004, 4, 337−348.

(13) Niemz, A.; Ferguson, T. M.; Boyle, D. S. Point-of-care nucleic acid testing for infectious diseases. *Trends Biotechnol.* 2011, 29, 240−250.

(14) Corman, V. M.; et al. Detection of 2019 novel coronavirus (2019-nCoV) by real-time RT-PCR. *Eurosurveillance* 2020, No. 2000045.

(15) King, D. P.; et al. Development of a TaqMan PCR assay with internal amplification control for the detection of African swine fever virus. *J. Virol. Methods* 2003, 107, 53−61.

(16) Notomi, T. Loop-mediated isothermal amplification of DNA. *Nucleic Acids Res.* 2000, 28, No. 63e.

(17) Piepenburg, O.; Williams, C. H.; Stemple, D. L.; Armes, N. A. DNA detection using recombination proteins. *PLoS Biol.* 2006, 4, No. e204.

(18) Tian, A. L.; et al. A novel recombinase polymerase amplification (RPA) assay for the rapid isothermal detection of Neospora caninum in aborted bovine fetuses. *Vet. Parasitol.* 2018, 258, 24−29.

(19) Tomita, N.; Mori, Y.; Kanda, H.; Notomi, T. Loop-mediated isothermal amplification (LAMP) of gene sequences and simple visual detection of products. *Nat. Protoc.* 2008, 3, 877−882.

(20) Goto, M.; Honda, E.; Ogura, A.; Nomoto, A.; Hanaki, K. Colorimetric detection of loop-mediated isothermal amplification reaction by using hydroxy naphthol blue. *Biotechniques* 2009, 46, 167−172.

(21) Yan, C.; et al. Rapid and visual detection of 2019 novel coronavirus (SARS-CoV-2) by a reverse transcription loop-mediated isothermal amplification assay. *Clin. Microbiol. Infect.* 2020, 26, 773−779.

(22) Xia, S.; Chen, X. Single-copy sensitive, field-deployable, and simultaneous dual-gene detection of SARS-CoV-2 RNA via modified RT-RPA. *Cell Discovery* 2020, 6, No. 37.

(23) James, H. E.; et al. Detection of African swine fever virus by loop-mediated isothermal amplification. *J. Virol. Methods* 2010, 164, 68−74.

(24) Miao, F.; et al. Rapid and Sensitive Recombinase Polymerase Amplification Combined With Lateral Flow Strip for Detecting African Swine Fever Virus. *Front. Microbiol.* 2019, 10, No. 1004.

(25) Tian, B.; Minero, G. A. S.; Fock, J.; Dufva, M.; Hansen, M. F. CRISPR-Cas12a based internal negative control for nonspecific products of exponential rolling circle amplification. *Nucleic Acids Res.* 2020, 48, No. e30.

(26) Rolando, J. C.; Jue, E.; Barlow, J. T.; Ismagilov, R. F. Real-time kinetics and high-resolution melt curves in single-molecule digital LAMP to differentiate and study specific and non-specific amplification. *Nucleic Acids Res.* 2020, 48, No. e42.

(27) Gootenberg, J. S.; et al. Nucleic acid detection with CRISPR-Cas13a/C2c2. *Science* 2017, 356, 438−442.

(28) Chen, J. S.; et al. CRISPR-Cas12a target binding unleashes indiscriminate single-stranded DNase activity. *Science* 2018, 360, 436−439.

(29) Li, S. Y.; et al. CRISPR-Cas12a-assisted nucleic acid detection. *Cell Discovery* 2018, 4, No. 20.

(30) Teng, F.; et al. CDetection: CRISPR-Cas12b-based DNA detection with sub-attomolar sensitivity and single-base specificity. *Genome Biol.* 2019, 20, No. 132.

(31) Li, S. Y.; et al. CRISPR-Cas12a has both cis- and trans-cleavage activities on single-stranded DNA. *Cell Res.* 2018, 28, 491−493.

(32) Abudayyeh, O. O.; et al. C2c2 is a single-component programmable RNA-guided RNA-targeting CRISPR effector. *Science* 2016, 353, No. aaf5573.

(33) Li, L.; et al. HOLMESv2: A CRISPR-Cas12b-Assisted Platform for Nucleic Acid Detection and DNA Methylation Quantitation. *ACS Synth. Biol.* 2019, 8, 2228−2237.

(34) Broughton, J. P.; et al. CRISPR-Cas12-based detection of SARS-CoV-2. *Nat. Biotechnol.* 2020, 38, 870−874.

(35) Wang, X.; et al. CRISPR/Cas12a technology combined with immunochromatographic strips for portable detection of African swine fever virus. *Commun. Biol.* 2020, 3, No. 62.

(36) Wang, B.; et al. Cas12aVDet: A CRISPR/Cas12a-Based Platform for Rapid and Visual Nucleic Acid Detection. *Anal. Chem.* 2019, 91, 12156−12161.

(37) Tao, D.; et al. Application of CRISPR-Cas12a Enhanced Fluorescence Assay Coupled with Nucleic Acid Amplification for the Sensitive Detection of African Swine Fever Virus. *ACS Synth. Biol.* 2020, 9, 2339−2350.

(38) Li, Y.; Mansour, H.; Wang, T.; Poojari, S.; Li, F. Naked-Eye Detection of Grapevine Red-Blotch Viral Infection Using a Plasmonic CRISPR Cas12a Assay. *Anal. Chem.* 2019, 91, 11510−11513.

(39) Zhang, W. S.; et al. Reverse Transcription Recombinase Polymerase Amplification Coupled with CRISPR-Cas12a for Facile and Highly Sensitive Colorimetric SARS-CoV-2 Detection. *Anal. Chem.* 2021, 93, 4126−4133.

(40) Cheng, X.; et al. CRISPR/Cas12a-Modulated fluorescence resonance energy transfer with nanomaterials for nucleic acid sensing. *Sens. Actuators, B* 2021, 331, No. 129458.

(41) Ding, X.; et al. Ultrasensitive and visual detection of SARS-CoV-2 using all-in-one dual CRISPR-Cas12a assay. *Nat. Commun.* 2020, 11, No. 4711.

(42) Chen, Y.; et al. Contamination-free visual detection of SARS-CoV-2 with CRISPR/Cas12a: A promising method in the point-of-care detection. *Biosens. Bioelectron.* **2020**, *169*, No. 112642.

(43) Barnes, K. G.; et al. Deployable CRISPR-Cas13a diagnostic tools to detect and report Ebola and Lassa virus cases in real-time. *Nat. Commun.* **2020**, *11*, No. 4131.

(44) Joung, J.; et al. Detection of SARS-CoV-2 with SHERLOCK One-Pot Testing. *N. Engl. J. Med.* **2020**, *383*, 1492−1494.

(45) Fozouni, P.; et al. Amplification-free detection of SARS-CoV-2 with CRISPR-Cas13a and mobile phone microscopy. *Cell* **2021**, *184*, 323.e9−333.e9.

(46) Zhao, C.; et al. CRISPR-offinder: a CRISPR guide RNA design and off-target searching tool for user-defined protospacer adjacent motif. *Int. J. Biol. Sci.* **2017**, *13*, 1470−1478.

(47) CDC: Centers for Disease Control and Prevention. *Real-time RT-PCR Panel for Detection 2019-nCoV*; U.S. Centers for Disease Control and Prevention, 2020. https://www.cdc.gov/coronavirus/2019-ncov/lab/rt-pcr-detection-instructions.html.

(48) WHO: World Health Organization. *Diagnostic Detection of Wuhan Coronavirus 2019 by Real-Time RT-PCR*; World Health Organization, 2020. https://www.who.int/docs/default-source/coronaviruse/wuhan-virus-assay-v1991527e5122341d99287a1b17c111902.pdf.

(49) OIE: World Organization for Animal Health. *African Swine Fever (Infection with African Swine Fever)*; World Organization for Animal Health, 2019. https://www.oie.int/fileadmin/Home/eng/Health_standards/tahm/3.08.01_ASF.pdf.

(50) Liu, W. *SSD: Single Shot MultiBox Detector*; Springer: Cham, 2016; pp 21−37.

(51) Gulli, A.; Pal, S. *Deep Learning with Keras: Implement Neural Networks with Keras on Theano and TensorFlow*; Packt Publishing, 2017.

(52) Abadi, M.; Barham, P.; Chen, J.; Chen, Z.; Davis, A. et al. In *TensorFlow: A System for Large-ScaleMachine Learning*, Proceedings of the 12th USENIX Symposium on Operating Systems Designand Implementation (OSDI'16); USENIX Association, 2016.

(53) Fu, Y. A gene prioritization method based on a swine multi-omics knowledgebase and a deep learning model. *Commun. Biol.* **2020**, *3*, No. 502.

(54) Chollet, F. *Deep learning with Python*; Manning Publications: New York, 2018; Vol. *361*.

(55) Zhou, R.; Li, Y.; Dong, T.; Tang, Y.; Li, F. A sequence-specific plasmonic loop-mediated isothermal amplification assay with orthogonal color readouts enabled by CRISPR Cas12a. *Chem. Commun.* **2020**, *56*, 3536−3538.